

Ultrathin cobalt oxide films on Ir(100)-(1×1)

C. Giovanardi, L. Hammer, and K. Heinz*

Lehrstuhl für Festkörperphysik, Universität Erlangen-Nürnberg, Staudtstrasse 7, D-91058 Erlangen, Germany

(Received 6 June 2006; revised manuscript received 15 August 2006; published 29 September 2006)

We report on the formation of ultrathin Co oxide films by oxidation of correspondingly thin Co films epitaxially grown on the unreconstructed—i.e., metastable—(1×1) phase of Ir(100), on both the clean surface and the surface precovered with half a monolayer of oxygen. As investigated by low-energy electron diffraction patterns and intensities and by atomically resolved images from scanning tunneling microscopy (STM) the oxide forms mainly in its fcc-type rocksalt structure CoO. This is with exception of the submonolayer range and the surface precovered with oxygen for which the Co₃O₄ spinel-structured phase develops. Rather unusual, the CoO films appear in the polar (111) orientation and so, though the hexagons are slightly distorted, should become increasingly instable with growing thickness. However, STM images recorded under special conditions indicate that there are oxygen vacancies which lead to charge compensation and so may contribute to stabilize the (111) orientation. Also, STM retrieves a considerable buckling of cobalt layers which is inevitable when fcc(111) layers are accommodated on an fcc(100) substrate.

DOI: [10.1103/PhysRevB.74.125429](https://doi.org/10.1103/PhysRevB.74.125429)

PACS number(s): 68.47.Gh, 68.35.Ct, 68.37.Ef, 61.14.Hg

I. BACKGROUND

Recently it has been reported that the magnetic properties of epitaxial CoO films depend dramatically on the strain imposed by the supporting substrate.¹ The c/a ratio appears to play a crucial role with respect to the magnetocrystalline anisotropy which causes the easy magnetic axis to be oriented out of the film plane for CoO/MnO(100) (with $c/a < 1$) and in plane for CoO/Ag(100) (with $c/a > 1$). This is another example of the well-known intimate relationship between the magnetic and crystallographic properties of thin films. Surprisingly, there is also new work with new results on bulk CoO with respect to its crystallographic and magnetic structure. Though early work reported that the high-temperature fcc-rocksalt lattice transforms to the monoclinic lattice when the temperature is lowered below the Néel temperature (292 K)—i.e., to the antiferromagnetic state²—this was unambiguously proved by high-resolution x-ray studies only much later.³ Consistently, there are also both trigonal and tetragonal magnetic propagation vectors which were shown by neutron diffraction experiments only a few years ago.⁴ Also rather recently, the antiferromagnetism of CoO has been shown to be crucial for beating the superparamagnetic limit of small Co clusters by partial oxidation—i.e., embedding these clusters into a thin shell of surrounding CoO. The exchange bias involved has been reported to shift the limit from 10 K to as much as 290 K.^{5,6}

The recent work mentioned demonstrates that CoO is currently of high interest with respect to both its basic physical properties and its possible technological applications. Of special importance are epitaxial CoO films. They bear the potential to open new opportunities for applications in the field of exchange bias in multilayered magnetic systems by control of the strain through the choice of the substrate.¹ There are several investigations of epitaxial CoO films on different substrates as MnO(100),¹ MgO,⁷ Ag(100),^{1,8,9} and on bct(100) Co films epitaxially grown on Fe(100).¹⁰ All of them deal with the nonpolar (100)-orientated surface of CoO. The latter's (111)-oriented surface is polar and so suspicious

to be unstable as has been experienced by cutting a CoO bulk crystal along the (111) face. The surface stabilizes by reconstruction or by adsorption of impurities.¹¹ Alternatively, the surface was found to be covered by the second stable form of cobalt oxide—i.e., spinel-structured Co₃O₄—which was observed to form by mild oxidation of the (100) surface of a bulk CoO crystal.¹² Growth of CoO(111) by oxidation of the Co(0001) surface has been found to be stabilized by OH adsorption and to be of limited order.¹³ Thin epitaxial CoO(111) films prepared on Au(111) were assumed to be also stabilized by OH adsorption.¹⁴ This seems to be in contrast to CoO(111) films grown on Pt(111) which were claimed to be stable as clean and unreconstructed phases up to a coverage of six monolayers (6 ML).¹⁵ Cobalt oxide islands in (111) orientation were observed to grow on Ag(100), yet it could not be decided whether they originate from CoO or from Co₃O₄.⁹

In the present paper we report that ultrathin CoO(111) films can also be formed on an fcc(100) substrate, here Ir(100)-(1×1). Only at Co submonolayer coverage does oxidation lead to small patches of the more oxygen-rich spinel-type Co₃O₄ which, however, grow in size when the surface has been precovered with oxygen. For the polar film orientation we will show by scanning tunneling microscopy (STM) and low-energy electron diffraction (LEED) including intensity versus energy spectra, $I(E)$, that thin oxide films are reconstructed consistent with the accommodation of fcc(111) layers on an fcc(100) substrate and, accordingly, exhibit a significant buckling. Also, STM images recorded under special tip conditions indicate that there are oxygen vacancies. Both the latter and the buckling may account for the stability of the polar film orientation.

II. EXPERIMENT

The experiments were carried out in a two-stage UHV apparatus with a vessel hosting a homemade four-grid LEED optics and one hosting a commercial beetle-type STM (RHK) with easy transfer between the two stages. The sub-

strate surface Ir(100) is—in its stable phase—characterized by a complex quasihexagonal reconstruction Ir(100)-(5×1)-hex.¹⁶ However, this can be lifted by oxygen adsorption by which a (2×1) superstructure on the (1×1)-ordered substrate results. After chemical reduction by hydrogen, an almost bulklike-terminated and clean (1×1) phase is observed^{16–18} which, of course, is metastable.

The preparation of cobalt oxide films was realized in a two-step procedure—i.e., by deposition of Co on the surface and subsequent oxidation. The deposition was made both on the clean substrate and the surface precovered with half a monolayer of atomic oxygen, by which it exhibits the above-mentioned (2×1) superstructure Ir(100)-(2×1)-O, in agreement with the literature.¹⁹ Oxides of 1-ML and 2-ML Co films could be prepared by high-temperature post-oxidation. Full oxidation of 4 ML Co was only successful either by deposition of Co under simultaneous O₂ flux at 50 °C followed by additional high-temperature post-oxidation or by sequential deposition and post-oxidation of 2 ML Co.

For the metal deposition an electron-beam evaporator supplied with highly purified Co was used and operated at a deposition rate of about 0.2 ML/min. During operation and even during the deposition process the pressure in the UHV apparatus was below 10⁻¹⁰ mbar. Sample annealing, as necessary to allow for well-ordered Co films as well as for their oxidation, was accomplished via electron bombardment from the rear. Exposure of the metal films to oxygen was made by a doser positioned right in front of the sample. We estimate that the local gas pressure is about two orders of magnitude larger than the measured background pressure. The exposures given below correspond to this estimation.

In order to get LEED patterns with only little thermal diffuse intensities the sample was cooled by direct contact to a liquid-nitrogen reservoir while STM images, on the other hand, could be recorded only at room temperature. LEED intensity spectra were used as fingerprints to characterize both the development of the oxide as well as the fully developed oxides of different thicknesses. They were taken with the sample at about 90 K and by use of a 12-bit digital charge-coupled-device (CCD) camera whereby the video signal is evaluated under computer control.²⁰ The spectra recorded for the pure metal films on the clean substrate were identical to those measured earlier. According to the latter's quantitative full dynamical analyses the films are strictly pseudomorphic and are, as expected, tetragonally distorted normal to the surface (the distortion amounts to -18% for a 4-ML Co film²¹). Additionally, STM investigations of this earlier work show that at a coverage corresponding to the completion of a monolayer the films are practically flat, indicative of layer-by-layer growth.

In order to find the proper post-oxidation conditions for the Co films they were exposed to different amounts of oxygen at different temperatures. The development of the LEED patterns and the intensities of the (11) diffraction spot is shown in Fig. 1 for the oxidation of 2 ML Co. The exposure to oxygen and the annealing temperature were increased stepwise starting with the pure epitaxial 2-ML Co film grown on clean Ir(100)-(1×1). As obvious, the spectra and patterns are fully developed only when the exposure to oxygen

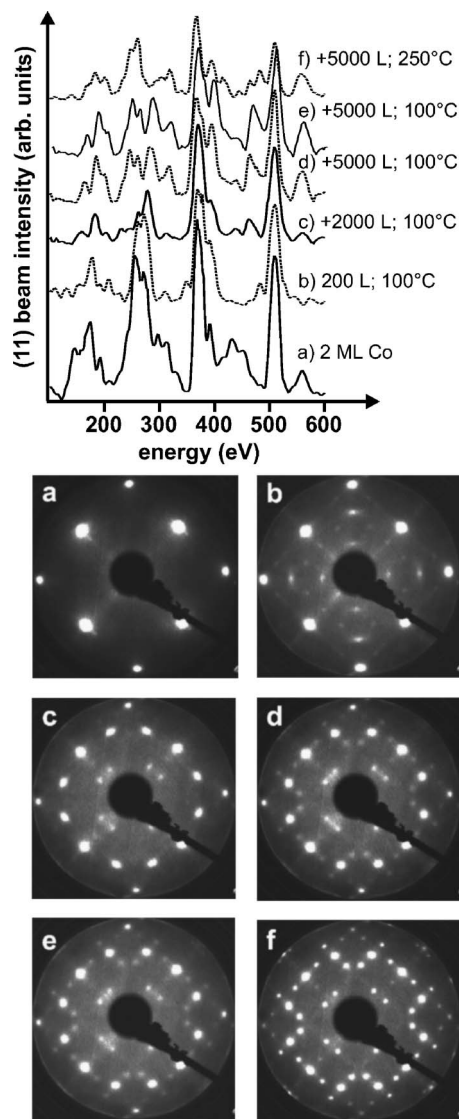


FIG. 1. Development of LEED spectra (11 beam) and LEED patterns (100 eV) upon oxidation of a 2-ML Co film grown on Ir(100)-(1×1). The various patterns correspond to different oxidation conditions—i.e., incremental exposures to oxygen and annealing temperatures as indicated in the top panel.

amounts to as much as 3000 L and the annealing temperature is as high as 250 °C [similar annealing temperatures were reported to be necessary for oxide formation on Ag(100) by Co deposition in an oxygen atmosphere.⁹] Obviously only then is the metal film fully oxidized. Consequently, for the post-oxidation of the metal already deposited the film was always exposed to 3000 L at a sample temperature of 250 °C. This applies also to the 1-ML Co film. As already mentioned thicker oxide films could only be produced by either Co deposition under O₂ flux or by incremental Co deposition followed by post-oxidation after each step.

III. RESULTS

A. CoO(111) films on Ir(100)-(1×1)

In Fig. 2, LEED patterns and STM images are displayed for the oxides resulting from oxidation of 1-, 2-, and 4-ML

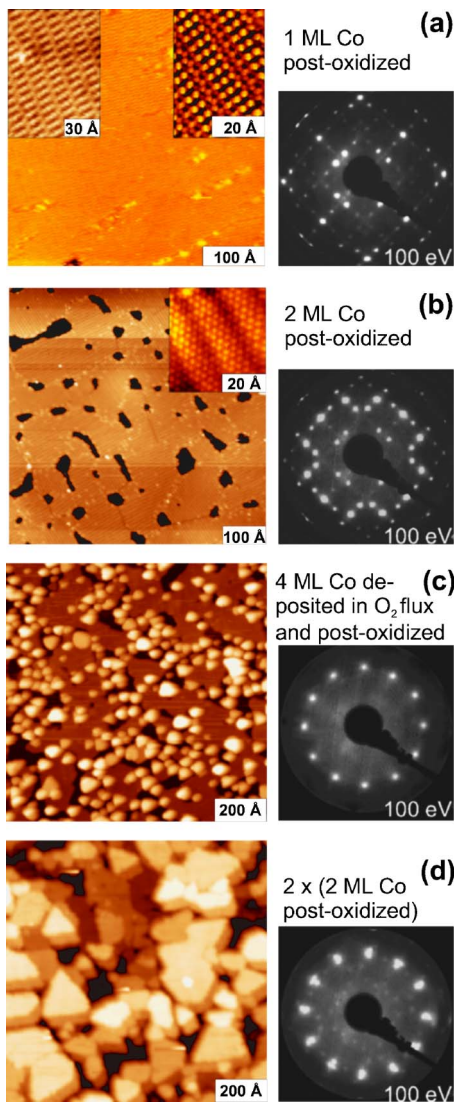


FIG. 2. (Color online) STM images and LEED patterns as resulting from full oxidation of Co films at coverage values of 1, 2, and 4 ML Co. STM image parameters are (a) 240 mV, 1.9 nA (left inset, 180 mV, 1.9 nA; right inset, 2.1 mV, 6.5 nA); (b) 1.65 V, 2.0 nA (inset: 150 mV, 2.0 nA); (c) 1.9 V, 0.63 nA; (d) 0.59 V, 0.55 nA.

Co films according to the procedures described in the last section. The large-scale images in panels (a) and (b) show that the oxide films resulting from $n=1$ ML and $n=2$ ML Co exhibit at most three height levels, indicating that there are holes in the layer n and some islands in the $(n+1)$ layer corresponding to approximate layer-by-layer epitaxial growth. Nevertheless, the zoom-in insets in the images resolve that on the atomic scale the films are rather buckled. On the other hand, the LEED patterns of these phases are rather complex. In contrast, the pattern of the 4-ML oxide film [Fig. 2(c)] exhibits only (nearly) hexagonally arranged LEED spots appearing in two domains rotated by 90° with respect to each other. There are no spots of quadratic order; i.e., at that thickness of the film the primary beam fails to reach the Ir(100) substrate with sufficient intensity. So the emerging diffraction spots stem from the oxide only. Evalu-

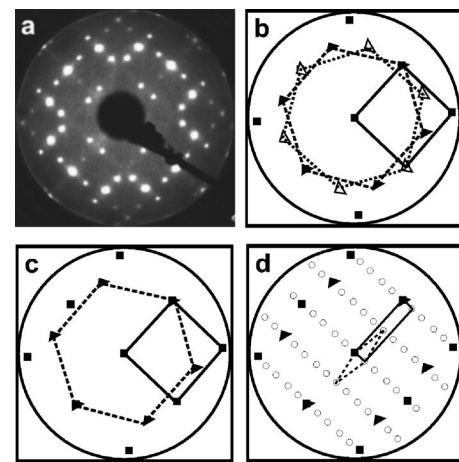


FIG. 3. Interpretation of the $c(10\times 2)$ LEED pattern (see text).

ation of the reciprocal lattice vectors supplies a real-space hexagonal unit mesh length of about 3.1 Å whereby, however, the hexagon appears to be slightly distorted (quasihexagon). The 4-ML Co oxide film prepared stepwise by subsequent deposition and oxidation of 2 ML Co in each step leads to a rough surface [Fig. 2(d)] with the LEED pattern exhibiting faint spots of quadratic order, the hexagonal spots, and additional such spots in split positions.

Quasihexagonally arranged spots are also part of the diffraction patterns of the 1- and 2-ML films [Figs. 2(a) and 2(b)] though more clearly visible at 2 ML [note that the sample is slightly rotated with respect to its orientation in Fig. 2(c)]. The corresponding LEED pattern is repeated in Fig. 3(a) and in the schematic pattern of Fig. 3(b) the spots originating from the quadratic substrate and the quasihexagonal spots only are displayed—equivalent to a pattern with no multiple diffraction between substrate and film involved. As the film spots stem from two domains mutually rotated by 90° , the pattern resulting from only one such domain is displayed in Fig. 3(c). The additional spots in the real LEED pattern originate from multiple (at least double) diffraction between quadratic and quasihexagonal layers. Usually, these multiple diffraction spots are the weaker the higher the layer diffraction orders involved. The full arrangement of spots for one domain is displayed in Fig. 3(d) [for comparison with experiment in panel (a) the spots of the other domain must be superimposed]. The diffraction pattern corresponds to a $c(10\times 2)$ superstructure as indicated by the centered and primitive unit meshes also given in Fig. 3(d).

According to Fig. 2(a) the LEED pattern for the 1-ML film has the same $c(10\times 2)$ symmetry, though—not surprisingly because of the different thickness of the oxide—the intensities are different. So we need for both films an atomic model accounting for the $c(10\times 2)$ LEED pattern as well as for the considerable atomic buckling resolved by STM. As already mentioned there are two stable bulk phases of cobalt oxide—i.e., the fcc-type rocksalt structure of CoO and the cubic spinel structure of Co_3O_4 . In the latter oxygen ions form an fcc lattice in which the cobalt ions assume both octahedral (Co^{3+}) and tetrahedral (Co^{2+}) interstitial sites. Only in the (111)-oriented layers of CoO and Co_3O_4 are

hexagonal arrangements of ions as required to form the LEED patterns observed. CoO appears to fit the experimental findings best: In its hexagonal oxygen or cobalt (111) layers (bulk lattice parameter 4.26 \AA) the nearest-neighbor spacing between atoms is $a_{\text{CoO}}=3.01 \text{ \AA}$ while that in the quadratic Ir layers is $a_{\text{Ir}}=2.715 \text{ \AA}$. So only little distortion is necessary for a structural coincidence mesh according to $10a_{\text{Ir}}=9a_{\text{CoO}}$ which cause the tenfold superperiodicity observed in the $[0\bar{1}1]$ direction. The corresponding ball model for the quasi-hexagonal layer at the interface (either oxygen or cobalt ions) is given in Fig. 4(a) for cobalt ions and the hollow-bridge registry as an example (alternatively the registry could be the bridge top). The quasi-hexagonal unit mesh, the substrate's quadratic unit mesh, and the centered and primitive $c(10 \times 2)$ superstructure unit meshes are inserted. In order to fit to the twofold superperiodicity in the $[011]$ direction the hexagon has to be slightly distorted with the unit mesh vectors enclosing an angle of $\arctan(\frac{9}{5})=60.95^\circ$ rather than the ideal 60° angle. The two vectors of the quasi-hexagonal unit mesh are of lengths $(10/9)a_{\text{Ir}} \approx 3.02 \text{ \AA}$ and $(\sqrt{106}/9)a_{\text{Ir}} \approx 3.11 \text{ \AA}$ —i.e., expanded with respect to the ideal hexagonal unit vectors by only 0.3% and 3.3%, respectively.

Due to the accommodation of a hexagonal layer on a quadratic one, a considerable buckling of the interface adlayer has to be expected and, indeed, the STM image of the 1-ML Co oxide displayed in Fig. 4(b) clearly is in line with that exhibiting a buckling amplitude of about 0.5 \AA as retrieved from the profile given in panel (c). Certainly, the buckling amplitude will depend on the registry of the interface ions with respect to the top substrate layer, as well as on the radius of the ions involved (cobalt or oxygen), and on what the STM “sees”—i.e., either the top layer of the oxide bilayer or that below. Of course, the answers to these questions are essential also for the interpretation of the 2-ML Co oxide whose STM image is displayed in Fig. 4(e) exhibiting a buckling amplitude of only about 0.1 \AA as taken from the profile in panel (f).

Addressing first the question of what the STM “sees” we have to consider that we tunnel to unoccupied states as there is a positive sample bias. STM measurements of the (100) surface of bulk CoO accompanied by first-principles calculations retrieved that at positive sample bias tunnelling is into empty Co $3d_{xy}$ states.²² On the other hand, detailed STM calculations for an FeO monolayer Pt(111) (Ref. 23) have shown that the STM image contrast is not directly related to the surface topography. So, e.g., maxima are over O positions for a Pt terminated tip but over Fe positions when the tip is O terminated. Generally, both Fe and O orbitals are involved in the tunneling-current formation whereby destructive interference can take place. For cobalt oxide films formed on Ag(100) the STM current was explained with tunneling through the oxide's band gap with a strong bias-voltage dependence for CoO(100) structures.⁹ Oxide patches with (111) orientation (for which it could not be decided whether they were CoO or Co_3O_4 type) exhibited a less strong voltage-dependent contrast and no clear band gap. Obviously, the tunnel current formation for thin oxide films is very complex so that the quantitative interpretation of

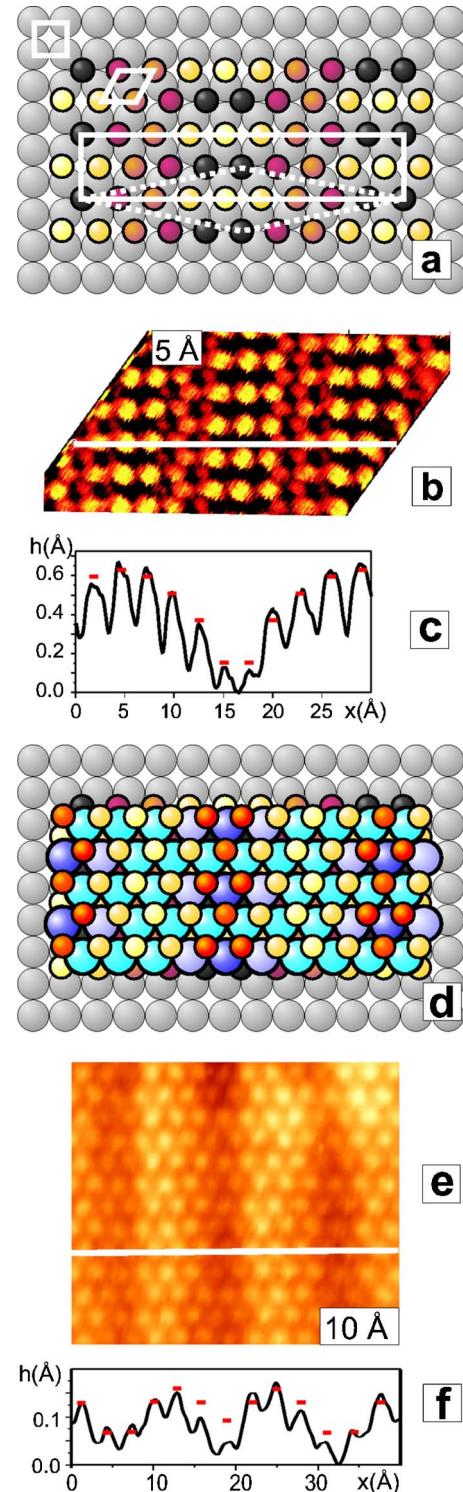


FIG. 4. (Color online) Ball models of a single cobalt ion adlayer (a) and a Co-O-Co trilayer (d) both in $c(10 \times 2)$ order with respect to the Ir(100) substrate. The panels below the ball models display the atomically resolved STM images of the 1-ML Co oxide [(b) $+2.1 \text{ mV}$, 6.5 nA] and of the 2-ML Co oxide [(e) $+150 \text{ mV}$, 2.0 nA] together with the corresponding buckling profiles (c), (f) along the line inserted in each case. The horizontal bars in panels (c), (f) indicate the atomic heights calculated from the respective ball models.

STM profiles is only safe when based on calculations for the very system under consideration which, however, are lacking for the present case.

Fortunately, yet, the tunneling images provide rich information. As obvious from the image of the 1-ML Co oxide [Fig. 4(b)] and the profile below there is a wavelike buckling pattern in the $[0\bar{1}1]$ direction with a period characterized by three strong protrusions, followed on both sides by one at intermediate height (vertically in a zigzag arrangement) and another four at low height. In neighboring rows this pattern repeats with a phase shift equivalent to half of the long $c(10\times 2)$ unit mesh length. Both the buckling pattern and the phase shift are characteristic of the 1-ML oxide. The image and profile for the 2-ML oxide [Figs. 4(e) and 4(f)] are different from that; i.e., the buckling amplitude is much reduced, the height sequence is different, and there is only a small phase shift between the profiles of neighboring rows. Certainly, any geometric model for the oxides involved must be consistent with all these characteristics. Therefore, we have constructed hard-ball models for the different structural possibilities—i.e., cobalt or oxygen ions at the interface with bridge-hollow or bridge-top registry. Additionally, as the number of oxide ions in the unit cell is 9—i.e., uneven—we had to differentiate in each case whether there is an ideal bridge position with never an ideal hollow or top position possible or vice versa. The calculations assumed the CoO-specific ionic radii $r_{\text{Co}^{2+}}=0.88$ Å and $r_{\text{O}^{2-}}=1.25$ Å. As a result, we can clearly identify a single model: Only for Co ions at the interface in bridge-hollow registry (with ideal bridge sites) and assuming that we tunnel indeed to Co states in both the 1-ML and 2-ML Co oxide are all features of the experimental STM data reproduced.

Figure 4(a) displays this situation. The shading (coloring) of the atoms is according to their height [dark, almost hollow positions; bright (yellow and dark yellow), bridge and almost bridge positions; grey (red and orange), positions intermediate between bridge and hollow]. Evidently, the height sequence of the protrusions of the experimental STM image is fully reproduced including the phase shift between neighboring rows and the vertical zig zag arrangement of protrusions of intermediate height. The calculated height of the ions is inserted in the profile in Fig. 4(c) as horizontal bars (total buckling amplitude 0.47 Å). Given the sensitivity of STM to electronic features, the agreement with the pure geometry is surprisingly good. This holds also for the 2-ML oxide whose geometry (again with the top oxygen layer missing) is displayed in Fig. 4(d). As for the 1-ML case all features of the STM image and the height of protrusions are reproduced (total buckling amplitude 0.10 Å). The reproduction of all details of the STM images makes us confident that the models given in Figs. 4(a) and 4(d) are correct.

At four CoO bilayers the oxide film thickness amounts to about 12 Å. As already mentioned, electron attenuation therefore largely prohibits the transfer of structural information from the substrate back to the surface—in line with the strong weakening of substrate spots in the LEED pattern of Fig. 2(c). Surprisingly, the two differently prepared oxides differ by the appearance in LEED and STM. While the oxide prepared under O_2 flux followed by post-oxidation exhibits

quasihexagonally arranged LEED spots as also part of the $c(10\times 2)$ pattern, there are additional spots in the stepwise-formed 4-ML oxide [Fig. 2(d)]. Evaluation of the pattern shows that these spots result from a lateral relaxation of the CoO layer so that it assumes its bulklike parameters with respect to both the ideal 60° hexagon and the ideal 3.01-Å unit mesh length. The rotational relaxation can be in both directions so that additional to the two orthogonal domains another two domains appear for each orientation. As obvious from the persistence of the quasihexagonal spots the relaxation does not apply to the full oxide film but only part of it, presumably the oxide layer(s) added in the second step of the preparation. The STM image tells that the respective surface is considerably rougher than that of the 4-ML Co film oxidized in one step. This indicates that once the first distorted CoO(111) film has been formed further deposition of Co and subsequent oxidation leads to three-dimensional (3D) type rather than layerwise growth.

B. Oxide formation under increased exposure to oxygen

The oxidation procedures applied so far resulted always in oxide films with the (distorted) CoO rocksalt structure, even when oxygen was supplied already during Co deposition. Another way to increase the relative amount of oxygen is to decrease the amount of available Co—i.e., to post-oxidize a Co film of submonolayer coverage. Alternatively, the Co deposition can be made on the surface precovered with half a monolayer oxygen [Ir(100)-(2×1)-O phase] followed by post-oxidation. Of course, submonolayer deposition can also be on the oxygen precovered surface. All three procedures were tested.

1. Oxides from submonolayer Co films on the clean and oxygen precovered substrate

When a Co film below but close to 1 ML is deposited on clean Ir(100) and subsequently oxidized domains with the CoO(111)-typical $c(10\times 2)$ superstructure appear with, however, small islands of different symmetry and a striped structure built in [Fig. 5(a)]. As resolved in the STM they appear at a height of 0.5 Å above the $c(10\times 2)$ phase with the stripes running at an angle of 45° with respect to the latter's unit mesh length axis. They own a periodicity of about 5.7 Å which is atypical for CoO. This structure is developed in much larger areas for an oxide resulting from deposition of a submonolayer of Co on the oxygen precovered surface, Ir(100)-(2×1)-O, and subsequent (further) oxidation [Fig. 5(b)]. For this preparation the new structure dominates, so that the LEED pattern recorded in parallel is characteristic of it. As given in Fig. 5(c) it exhibits a (3×3) superstructure whereby weak additional hexagonal spots presumably come from small hexagonal domains.

The requirement to find an atomic model accounting for a (3×3) unit cell and the about 5.7-Å periodicity observed in the STM is met by assuming a $\text{Co}_3\text{O}_4(100)$ film accommodated on the surface. The spinel structure with its cubic unit-cell length of $a_{sp}=8.08$ Å is made up of an fcc sublattice of O^{2-} ions with lattice parameter $a_{\text{O}}^{\text{fcc}}=a_{sp}/2=4.04$ Å. Co^{2+}

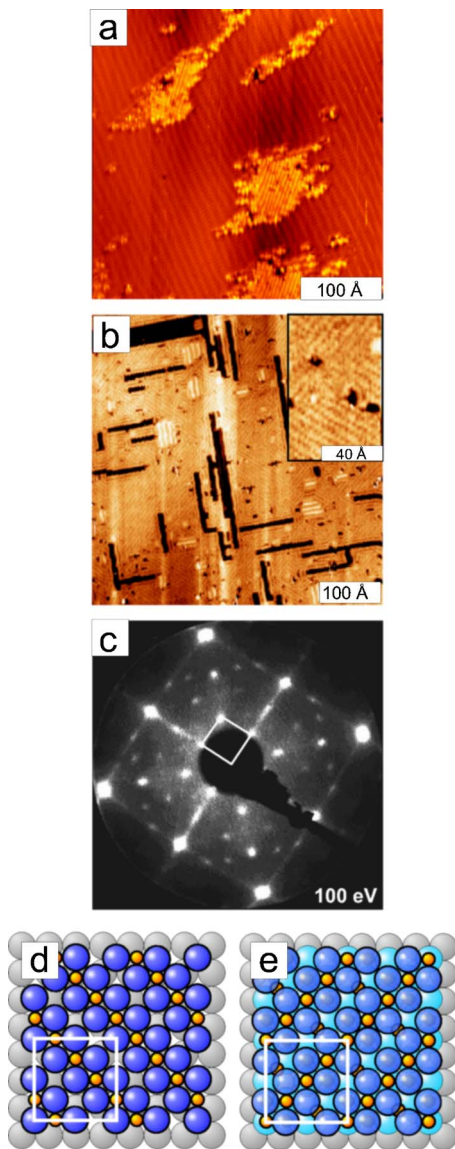


FIG. 5. (Color online) STM images resulting from oxidation of a submonolayer Co film deposited on (a) the clean Ir surface (2.25 V, 6.8 nA) and (b) the oxygen precovered surface [25 mV, 1.9 nA (same for inset)]. Panel (c) shows the LEED superstructure pattern of phase (b) with the unit (3×3) cell inserted, and (c),(d) present ball models accounting for that.

ions are accommodated in (1/8 of the available) tetrahedral sites of the oxygen lattice, Co^{3+} ions in (1/2 of the available) octahedral sites. As a consequence, in (100) orientation layers with quadratically ordered O^{2-} ions containing half as much Co^{3+} ions alternate with quadratically ordered Co^{2+} ions. In Fig. 5(d) a mixed layer is accommodated pseudomorphically on Ir(100). According to the model, $2a_{\text{O}}^{\text{fcc}} = 8.08 \text{ \AA}$ is expanded to $3a_{\text{Ir}} = 8.15 \text{ \AA}$; i.e., the spinel lattice needs to be distorted by only 0.8%. As observed in LEED there is a (3×3) superperiodicity. Moreover, assuming that the tunneling is still to cobalt ions the STM should see rows with a periodicity of $3a_{\text{Ir}}/\sqrt{2} = 5.76 \text{ \AA}$, again in close agreement with experiment. This holds also with further growth of this phase: the next layer would be made up of rows of Co^{2+}

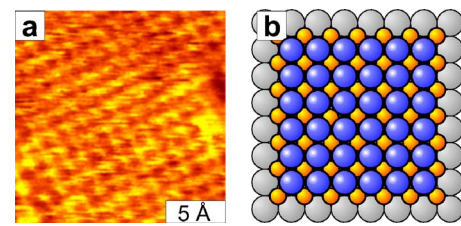


FIG. 6. (Color online) STM image of occasionally found (1×1) domains (100 mV, 2.2 nA).

ions followed again by a mixed layer as displayed in Fig. 5(e). The extent to which the model meets experiment strongly favors that under the oxygen-rich preparation conditions described in fact a spinel phase grows on Ir(100). It also supports our above assumption that tunneling is to cobalt ions as only those (in contrast to oxygen ions) are arranged in rows of 5.7-\AA spacings.

Occasionally, we found also small islands appearing as a (1×1) phase in the STM as displayed in Fig. 6(a). We interpret this as such a $\text{CoO}(100)$ layer as illustrated in Fig. 6(b) though the strain imposed by the substrate is rather large (9.9%). Concerning the latter one should note that for a single oxide bilayer this strain can be released by appropriate vertical relaxations.

2. Oxide from a 2-ML Co film deposited on the oxygen precovered substrate

As shown in the last section the oxidation of submonolayer Co films under oxygen-rich conditions favors the growth of spinel-type cobalt oxide, which owns 1/3 more oxygen than rocksalt-type CoO . Seemingly, the substrate precovered with half a monolayer oxygen is crucial for the development of extended Co_3O_4 domains. So the question arises whether or not this precoverage is sufficient to oxidize also thicker Co films in the spinel structure. Yet, as evident from Fig. 7(a), the STM image resulting from the corresponding preparation of a 2-ML film is very much similar to that arising from the 1-ML Co film deposited on the clean surface and subsequently oxidized. There is the 1-ML- $\text{CoO}(111)$ -typical row-to-row phase shift of surface buckling, in spite of the fact that we are dealing with a 2-ML Co oxide film. In agreement with a $\text{CoO}(111)$ phase the LEED pattern exhibits the $c(10 \times 2)$ superstructure [Fig. 7(b)].

In contrast to STM, LEED electrons probe—though limited by attenuation—all surface layers and so the diffraction intensities provide a fingerprint of the full surface structure. Therefore, we compare in Fig. 7(c) spectra of two selected beams for the 2-ML Co oxides as prepared by deposition on the oxygen precovered surface with those for the 1-ML and 2-ML oxides prepared by Co deposition on the clean surface. As obvious, the spectra of all three phases are rather different. First, this shows unequivocally (as expected) that the 2-ML oxide prepared on the oxygen precovered surface is in fact different from the 1-ML oxide prepared on the clean surface in spite of their similar appearance in the STM. Second, it reflects that the structures of the two 2-ML oxides must be different, too. We can safely exclude that a spinel-

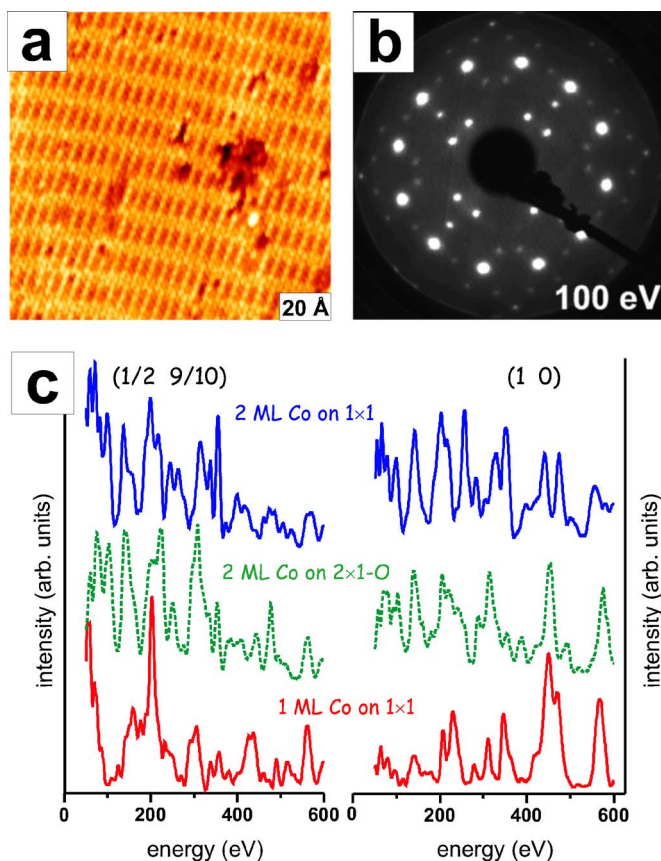


FIG. 7. (Color online) Data for the oxide resulting from 2 ML Co deposited on Ir(100)-(2×1)-O: (a) STM image (140 mV, 3.6 nA), (b) $c(10\times 2)$ LEED pattern, and (c) LEED intensities of two selected beams in comparison to the corresponding data of other phases.

type oxide layer is involved as this would cause additional (3×3) superstructure spots which, however, are lacking possibly due to insufficient oxygen supply. As a consequence, only CoO-type layers should form the film. The surface corrugation appearing in the STM is characteristic for a single Co(111) bilayer arranged on a quadratic layer. In principle, the latter could be a pure Co layer epitaxially grown on the Ir(100) substrate. Yet this is rather unlikely in view of the fact that the iridium surface had been precovered by half a monolayer of oxygen. The only valid interpretation we see is that the interface oxide is a CoO(100) layer in pseudomorphic (1×1) arrangement with the substrate, as already proposed for the small (1×1) domains found in the submonolayer regime. As further growth of CoO(100) layers is unfavorable because of the large lattice strain involved, the rather unstrained CoO(111) bilayer forms on top of the CoO(100) bilayer.

IV. DISCUSSION AND CONCLUSION

As demonstrated, our LEED and STM data strongly suggest that oxidation of up to 4 ML Co epitaxially grown on Ir(100) leads mainly to rocksalt-structured CoO films in the polar (111) orientation though the unequivocal crystallo-

graphic proof for that—e.g., by a quantitative LEED analysis—is still to come. The methods applied provide no direct information on the film stoichiometry or the related oxidation state of Co but only reveal the basic type of the oxide formed. The rocksalt-type CoO seems to be established even when the Co film is deposited under the simultaneous flux of O_2 directed on the sample. Only under special oxygen-rich conditions, as realized by the substrate precovered with half a monolayer of oxygen and by reducing the amount of available cobalt during oxidation (submonolayer coverage), are there patches which can be interpreted as (100)-oriented domains of the Co_3O_4 spinel structure.

The polar CoO(111) orientation derived deserves some further discussion in view of the well-known fact that bulk-terminated polar surfaces must be unstable due to the divergence of the electrostatic energy with growing sample thickness.²⁴ As described in the literature (see, e.g., review in Ref. 25) stabilization—i.e., suppression of the divergence—comes only by (a) chemical restructuring of one or several surface layers changing the surface chemistry, (b) adsorption of impurities carrying appropriate charges, or (c) electron redistribution in the whole sample including the filling of surface states or combinations of these effects. They all must provide additional surface charges so that the macroscopic dipole moment due to the adding up of bilayer dipoles constituting the sample is canceled (“charge compensation”). Indeed, a chemical, so-called octopolar (2×2) reconstruction, has been reported for the NiO(111) single-crystal surface^{26,27} and for NiO(111) films grown on Au(111) (Ref. 28) and on Ni(111) (Ref. 29). For isostructural MgO(111) the octopolar reconstruction has been found only for oxygen termination and the surface prepared under oxygen-rich conditions, while in the other case combinations of several Mg-covered terminations with an anomalous filling of surface states are involved according to the mechanism (c) mentioned above.³⁰ Charge compensation by hydroxyl adsorption is also observed, and it appears that this surface is even more stable than the (100) orientation.³¹ Also, transition-metal deposition has been reported to account for charge compensation with a surface band filling involved (e.g., Ref. 32). For CoO(111) to our knowledge no chemical reconstruction has been retrieved. Instead and as cited already in the Introduction, hydroxyl group adsorption is the main mechanism for charge compensation.^{13,14,33}

Certainly any of the above-mentioned mechanisms would reduce the energy of our CoO(111) system. Yet as we deal with ultrathin oxide films there is no divergence of the dipole energy on the one hand and there are additional possibilities to reduce energy on the other hand. So a contraction of layer spacings reducing the dipole length may be active, possibly accompanied by an increase in bond covalency which makes the dipole moment decrease further. Also, as has been shown for an ultrathin NaCl(111) film on Al(111),³⁴ image charges possibly built up in the supporting metal can play a role as well as an increased stability of oxide layers with ionic charges reduced in comparison to the corresponding bulk oxide layers.

We cannot exclude any of these mechanism as we have no quantitative experimental or computational information about the layer spacings and the charges accommodated on

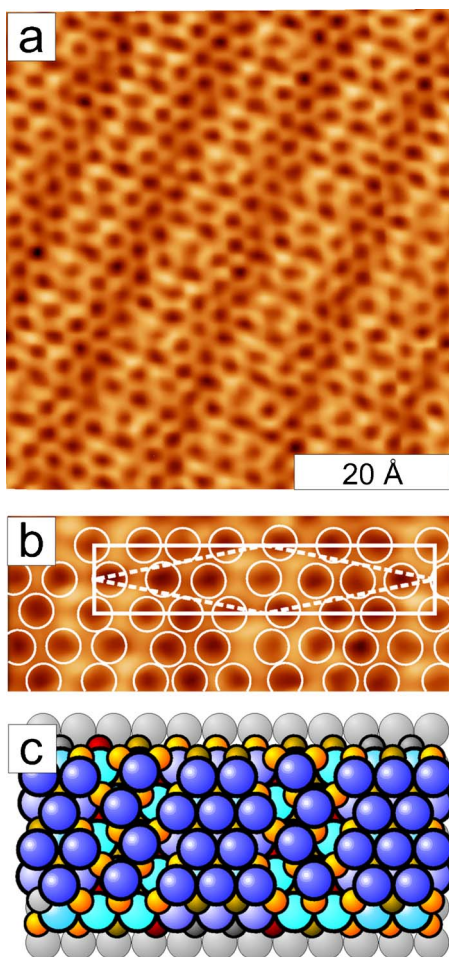


FIG. 8. (Color online) (a) Occasionally recorded STM image (6.4 mV, 4.7 nA) for a post-oxidized 2-ML Co film exhibiting surface depressions as encircled in the rotated part (b). They can be interpreted as oxygen ions as illustrated in the ball model (c).

the ions of the different oxide layers. Concerning hydroxyl contamination we note that the hydrogen residual gas pressure in our vessel was $<10^{-10}$ mbar and that for H_2O even less, much too small to allow for a significant surface contamination during the time of oxide preparation. Evenly unlikely is that the oxygen dosed on the surface has taken up hydrogen or water from the vessel's sides. However, we cannot exclude that our oxygen supply has been slightly contaminated so that by a sample exposure of several thousands Langmuir a monolayer contamination may result. Evidence is, however, that there is a strong buckling of cobalt layers which might influence the dipole moment. Even more important, yet, there are indications that the surface may in fact be chemically reconstructed with oxygen vacancies built in. Figure 8 presents one of occasionally recorded STM images which, however, were not reproducible, presumably due to accidental and rather undefined tip properties. Clearly and as illustrated in the rotated STM section in panel (b), there are seven depressions within the $c(10 \times 2)$ unit cell (instead of nine elevations observed under regular tunneling conditions). They are laterally not equidistant (as the elevations were), but form vertical stripes made up of triples and pairs of close spaced depressions separated with an enlarged spac-

ing by zigzag rows of single depressions. We speculate that the depressions are oxygen ions in the top layer resolved due to an irregular tip which, when regular, would detect cobalt ions [note that for $\text{FeO}(111)$ films a Pt tip which has taken up an oxygen atom “sees” oxygen ions²³]. With only seven oxygen ions there are two vacancies per primitive unit cell; i.e., the oxygen coverage in the top layer is only $7/9$. The vacancies might come by the loss of oxygen ions with a reduced bonding strength which in turn may come by the spatially varying binding caused by the buckled cobalt layer(s). Lateral relaxations after the formation of vacancies may account for the above-mentioned different spacings of the remaining ions. A corresponding ball model is displayed in Fig. 8(c) where zigzag rows of oxygen ions reside in hcp (instead of fcc) sites so that the free space formed by each oxygen vacancies is split into two halves. This model is in strong correspondence to the STM image in Fig. 8(b). In spite of this consistent scenario we have to stress that the presented interpretation of the STM image is not without speculations. Only further investigations including, e.g., tunneling spectroscopy and dynamical LEED intensity analysis may confirm our interpretation.

Interestingly, a $c(10 \times 2)$ superstructure as found in the present paper was also reported to be formed by high-temperature oxidation of 1 ML Fe deposited on the hexagonally reconstructed surface $\text{Pt}(100)\text{-hex-R}0.7^\circ$.³⁵ The hexagonal reconstruction was found to be lifted by the iron deposition, and a quantitative LEED analysis of the oxide film yielded the best theory-experiment fit for a buckled $\text{FeO}(111)$ double layer with iron at the interface and oxygen terminating the film. Thicker oxide films were attributed to the Fe_3O_4 structure. Later work of the same research group on the same system found that for the 1-ML iron oxide $c(10 \times 2)$ and (2×9) superstructures coexist on the surface.³⁶ The authors report that the LEED intensity analysis is of much better quality when based on the (2×9) phase, yet at the cost of the uniqueness of the result (two distinct best-fit structures were found). Again the surface is reported to be oxygen terminated with, however, the Fe-O layer spacing contracted by about 50% as compared to (111) layers of bulk FeO , a relaxation which was also reported for a (111)-oriented FeO layer grown on $\text{Pt}(111)$.³⁷ A quasi-hexagonal arrangement of oxide atoms on a quadratically ordered substrate was also found for the oxidized $\text{Rh}(100)$ surface.³⁸ Again there is a centered rectangular unit cell, in this case a $c(8 \times 2)$ one due to a slightly different ratio of substrate and oxide lattice parameters. Yet here both the interface layer and the surface terminating layer is formed by oxygen ions, equivalent to a O-Rh-O trilayer residing on the $\text{Rh}(100)$ substrate with the hexagon slightly distorted due to oxide's accommodation to the substrate. We assume that the different stoichiometry and interface structure compared to the present paper are due to the different stoichiometry and structure of bulk rhodium oxide, which is RhO_2 in rutile structure.

In conclusion we have found that ultrathin cobalt oxide films prepared by oxidation of ultrathin Co films epitaxially grown on $\text{Ir}(100)\text{-(}1 \times 1\text{)}$ consist dominantly of rocksalt-type CoO in the polar (111) orientation. Only in the submonolayer range of Co and with the surface precovered by oxygen does

the spinel-type phase Co_3O_4 develop. The hexagonal CoO unit mesh is slightly distorted so that there is a $c(10\times 2)$ coincidence mesh with respect to the quadratic substrate as clearly appearing in LEED. The accommodation of hexagonal to quadratic layers leads to a buckling of the interface cobalt ion layer which is well resolved in the STM. The stabilization of the polar orientation is—though we cannot

exclude contributions from other mechanisms—likely to come by oxygen vacancies in the top layer which produce the necessary charge compensation.

ACKNOWLEDGMENT

C.G. is indebted to the European Commission for support.

-
- *Corresponding Author. FAX: +49-9131-8528400. Electronic address: klaus.heinz@physik.uni-erlangen.de
- ¹S. I. Csiszar, M. W. Haverkort, Z. Hu, A. Tanaka, H. H. Hsieh, H.-J. Lin, C. T. Chen, T. Hibma, and L. H. Tjeng, *Phys. Rev. Lett.* **95**, 187205 (2005).
 - ²S. Saito, K. Nakahigashi, and Y. Shimomura, *J. Phys. Soc. Jpn.* **21**, 850 (1966).
 - ³W. Jauch, M. Reehuis, H. J. Bleif, F. Kubanek, and P. Pattison, *Phys. Rev. B* **64**, 052102 (2001).
 - ⁴K. Tomiyasu, T. Inami, and N. Ikeda, *Phys. Rev. B* **70**, 184411 (2004).
 - ⁵V. Skumryev, S. Stoyanov, Y. Zhang, G. Hadjipanayis, D. Givord, and J. Nogués, *Nature (London)* **423**, 850 (2003).
 - ⁶G. Palasantzas, S. A. Koch, T. Vystavel, and J. T. M. De Hosson, *Adv. Eng. Mater.* **7**, 21 (2005).
 - ⁷S. D. Peacor and T. Hibma, *Surf. Sci.* **301**, 11 (1994).
 - ⁸I. Sebastian and H. Neddermeyer, *Surf. Sci.* **454–456**, 771 (2000).
 - ⁹C. Hagendorf, R. Shantyr, K. Meinel, K.-M. Schindler, and H. Neddermeyer, *Surf. Sci.* **532–535**, 346 (2003).
 - ¹⁰S. Valeri, A. Borghi, G. C. Gazzadi, and A. di Bona, *Surf. Sci.* **423**, 346 (1999).
 - ¹¹C. Mocuta, A. Barbier, and G. Renaud, *Appl. Surf. Sci.* **162**, 56 (2000).
 - ¹²G. A. Carson, M. H. Nassir, and M. A. Langell, *J. Vac. Sci. Technol. A* **14**, 1637 (1996).
 - ¹³D. Cappus, M. Haßel, E. Neuhaus, M. Heber, F. Rohr, and H.-J. Freund, *Surf. Sci.* **337**, 268 (1995).
 - ¹⁴S. Sindhu, M. Heiler, K.-M. Schindler, and H. Neddermeyer, *Surf. Sci.* **541**, 197 (2003).
 - ¹⁵S. Entani, M. Kiguchi, and S. Koichiro, *Surf. Sci.* **566–568**, 165 (2004).
 - ¹⁶A. Schmidt, W. Meier, L. Hammer, and K. Heinz, *J. Phys.: Condens. Matter* **14**, 12353 (2002).
 - ¹⁷J. Küppers and H. Michel, *Appl. Surf. Sci.* **3**, 179 (1979).
 - ¹⁸K. Heinz, G. Schmidt, L. Hammer, and K. Müller, *Phys. Rev. B* **32**, 6214 (1985).
 - ¹⁹K. Johnson, Q. Ge, S. Titmuss, and D. A. King, *J. Chem. Phys.* **112**, 10460 (2000).
 - ²⁰K. Heinz, *Rep. Prog. Phys.* **58**, 637 (1995).
 - ²¹W. Meyer, C. Giovanardi, L. Hammer, and K. Heinz (unpublished).
 - ²²M. R. Castell, S. L. Dudarev, G. A. D. Briggs, and A. P. Sutton, *Phys. Rev. B* **59**, 7342 (1999).
 - ²³H. C. Galloway, P. Sautet, and M. Salmeron, *Phys. Rev. B* **54**, R11145 (1996).
 - ²⁴P. Tasker, *J. Phys. C* **12**, 4977 (1979).
 - ²⁵C. Noguera, *J. Phys.: Condens. Matter* **12**, R367 (2000).
 - ²⁶A. Barbier, G. Renaud, C. Mocuta, and A. Stierle, *Surf. Sci.* **433–435**, 761 (1999).
 - ²⁷A. Barbier, C. Mocuta, H. Kuhlenbeck, K. F. Peters, B. Richter, and G. Renaud, *Phys. Rev. Lett.* **84**, 2897 (2000).
 - ²⁸C. A. Ventrice, T. Bertrams, H. Hannemann, A. Brodde, and H. Neddermeyer, *Phys. Rev. B* **49**, 5773 (1994).
 - ²⁹F. Rohr, K. Wirth, J. Libuda, D. Cappus, M. Bäumer, and H.-J. Freund, *Surf. Sci.* **315**, L977 (1994).
 - ³⁰F. Finocchi, A. Barbier, J. Jupille, and C. Noguera, *Phys. Rev. Lett.* **92**, 136101 (2004).
 - ³¹K. Refson, R. A. Wogelius, D. G. Fraser, M. C. Payne, M. H. Lee, and V. Milman, *Phys. Rev. B* **52**, 10823 (1995).
 - ³²J. Goniakowski and C. Noguera, *Phys. Rev. B* **66**, 085417 (2002).
 - ³³M. Schönnenbeck, D. Cappus, J. Klinkmann, H.-J. Freund, L. G. M. Petterson, and P. S. Bagus, *Surf. Sci.* **347**, 337 (1996).
 - ³⁴W. Hebenstreit, M. Schmid, J. Redinger, R. Podlucky, and P. Varga, *Phys. Rev. Lett.* **85**, 5376 (2000).
 - ³⁵M. Ritter, H. Over, and W. Weiss, *Surf. Sci.* **371**, 245 (1997).
 - ³⁶S. Shaikhutdinov, M. Ritter, and W. Weiss, *Phys. Rev. B* **62**, 7535 (2000).
 - ³⁷Y. J. Kim, C. Westphal, R. X. Ynzunza, H. C. Galloway, M. B. Salmeron, M. A. Van Hove, and C. S. Fadley, *Phys. Rev. B* **55**, R13448 (1997).
 - ³⁸J. Gustafson *et al.*, *Phys. Rev. B* **71**, 115442 (2005).